Electronic Supplementary Material (ESI) for Physical Chemistry Chemical Physics.

Supporting Information

ZSM-5 Decrystallization and Dealumination in Hot Liquid Water

Alex R. Maag[†], Geoffrey A. Tompsett[†], Jason Tam[‡], Cheen Aik Ang[‡], Gisele Azimi[‡], Alexander D. Carl[†], Xinlei Huang,[§] Luis J. Smith[¥], Ronald L. Grimm[†], Jesse Q. Bond,[§] Michael T. Timko[,†]*

[†]Department of Chemical Engineering at Worcester Polytechnic Institute, 100 Institute Road, Worcester, Massachusetts 01609, USA

[‡]Department of Chemical Engineering and Applied Chemistry and Material Sciences and Engineering, University of Toronto, Toronto, Ontario M5S 3E5, Canada

[§]Department of Biomedical and Chemical Engineering, Syracuse University, 329 Link Hall, Syracuse, NY 13244

[¥]Department of Chemistry, Clark University, 950 Main Street, Worcester MA 01610, USA

The Supporting Information contains: 1) detailed descriptions of experimental methods; 2) additional nitrogen adsorption isotherms and analyses; 3) additional NMR data: 1D ^{29}Si NMR spectra and 2D Al MQMAS NMR spectra; 4) EDS images, 5) pyridine IR spectra; 6) kinetic analysis of time-dependent zeolite degradation data; 7) decrystallization and dealumination rate constants determined from the XRD and NMR data obtained in this study.

1. Detailed Experimental Protocol

1.1 Catalytic Packed Bed Setup

The catalytic packed bed setup used for ZSM-5 stability and activity studies consists of an AISI type 316 stainless steel Sitec tube (5.2 mm ID, 9.5mm OD) and peripheral equipment. The tube could hold approximately 0.5 grams of catalyst, and a 0.2 μm porous frit was press fit on one end of the tube to contain the zeolite powder. Both ends of the tube were pressure sealed into Sitec tees, which served as the inlet and outlet of the flow reactor. The entire assembly along with a section of stainless steel tubing (10 m × 0.1 cm i.d) was placed inside a temperature-controlled oven (HP 5890 gas chromatogram oven). Temperatures on the tube surface and inside both the inlet and outlet tees were logged to within ±1 °C using k-type thermocouples (Omega Engineering).

1.2 Batch Stability Measurements

A catalytic batch reactor setup was used to evaluate the hydrothermal stability of zeolite frameworks other than ZSM-5. Zeolites were purchased from Zeolyst, including frameworks HY (CBV-760, Si/Al = 30), Hβ (CP814C, Si/Al = 19), mordenite (CBV 21A Si/Al = 10), and ferrierite (CP914C, Si/Al = 10). Each was calcined at 550 °C in air prior to use. The batch reactor setup

consisted of a 300 ml AISI type 316 stainless steel Parr Reactor (Model 452HC2) and peripheral equipment. The batch reactor was loaded with 0.5 g of zeolite and 100 ml of deionized water, pressure sealed, and loaded into the reactor assembly. The reactor was initially pressurized to 2.7–10.3 MPa using N_2, which was varied to reach a pressure >25 MPa after heating. The reactor was constantly stirred with an impeller and heated to the desired temperature using an induction heater. The reactor temperature was logged to within ±1 °C using a J-type thermocouple (Omega Engineering). The total heat-up time was between 30-50 min and varied with the final temperature. The desired temperature of the zeolite and water mixture was maintained for three hours before quickly (~5 min) quenching the reaction with ice water. The reactor was then depressurized, the contents filtered to recover the zeolite, and the zeolite was dried in a 60 °C oven. The catalysts were characterized using X-ray diffraction described later in Section 1.3.

1.3 Catalyst Characterization

X-ray diffraction was performed using a Rigaku automatic instrument with the Bragg-Bretano theta-theta configuration. Diffractions were taken with a Cu Kα at 27.5kV and 5mA. Analysis was performed over the range from 5-80 2θ degrees with a 0.5° step size and 1 s dwell time. Crystallinity for each sample was determined from the sum of peak areas between 22.5-25 2θ degrees, as specified by ASTM method D5758-01.[1] The degree of crystallinity of a given sample was calculated from the ratio of these integrated peak areas of the treated sample to an untreated reference.

SEM images were captured using Hitachi SU8230 scanning electron microscope with a cold field emission source. The samples were mounted on the stub holder using carbon paste. No conductive coatings were applied to the specimens so that concurrent EDS measurements could provide composition data of the actual ZSM-5 surface.

Zeolite samples for STEM characterization were crushed using a mortar and pestle. The crushed powder was placed on a 200 mesh copper grid with a holey carbon support film. Secondary electron (SE), bright field (BF), and high angle annular dark field (HAADF) images were captured with a Hitachi HF-3300 microscope operated at an accelerating voltage of 300 kV.

Gas sorption was performed using an ASIQ iQ Quantachrome Instrument to determine surface area and micropore volume. Zeolite (0.025 g) was added to a glass bulb and the sample was degassed following a temperature ramp of 2 °C min^{-1} with 15-min temperature holds at 60, 80, 100 and 120 °C before increasing to 350 °C, where the temperature was maintained for 5 hours. The analysis procedure dosed nitrogen as the adsorbate into the sample cell cooled with liquid N_2 and obtained 60 isothermal P/P_0 points ranging from $5.5x10^{-7}$ to 1 followed by 15 desorption points between P/P_0 of 1 to 0.1. Micropore and external surface area were determined by applying the t-plot method to model the adsorption isotherm between P/P_0 of 0.15 to 1.

DRIFTS was performed using a Thermo Nicolet Magna 560 with a SpectraTech DRIFTS cell. The DRIFT cell was loaded with ZSM-5, and then purged with N_2 for 10 minutes. The temperature was increased in 20 °C increments at 10-15 min intervals until 100 °C, where it was held for 30 minutes before increasing in 50 °C increments until reaching 550 °C. Samples were analyzed over the range from 4000 to 600 cm^{-1}, at a resolution of 2 cm^{-1}, and an accumulation of 96 scans at 550 °C.

XPS was performed using a PHI Model 5600 MultiTechnique instrument controlled with AugerScan software. ZSM-5 samples were initially pelletized with a PIKE die kit and degassed prior to analysis. After introducing the sample, the chamber was evacuated to a pressure less than 5×10^{-9} Torr. X-rays from a monochromated Kα line at 1486.6 eV were directed towards the sample at 90° with respect to the analyzer. Survey scans were performed at 0.5 eV per step and 50 ms.

Sensitivity factors of 0.193 for Al 2p and 0.283 for Si 2p were used to obtain surface Si/Al ratios, as described previously.[2]

All ^{27}Al and ^{29}Si NMR spectra were collected at 9.4 T on a Varian INOVA spectrometer, using resonance frequencies of 104.17 MHz and 79.41 MHz, respectively. ^{29}Si data were collected using a 7.5 mm double resonance Chemagnetics MAS probe with a spinning rate of 4 kHz. A one-pulse experiment with a $\pi/6$ pulse at a pulse length of 2.1 μs and recycle delay of 12 s was used. All ^{29}Si spectra were referenced to the two chemical shifts in tetrakis(trimethylsilyl)silane (9.86 ppm and 135.34 ppm).[3] ^{27}Al data were collected using a 2.5 mm double resonance Chemagnetics MAS probe with a spinning rate of 20 kHz. A one-pulse experiment with a 1.0 μs long $\pi/6$ pulse and a 1.0 s recycle delay was used for the one-dimensional ^{27}Al spectra. Triple quantum ^{27}Al MQMAS experiments were conducted with the use of FAM-I conversion pulses[4] and a selective π pulse to generate a shifted echo for the purpose of whole echo data collection. An excitation pulse of 2.1 μs and a FAM-I sequence with four pulses, each with a pulse length of 0.6 μs, were used with a radio frequency field strength of 65 kHz. The selective π pulse had a pulse length of 4.8 μs using a radio frequency field strength of 35 kHz. The dwell time in the indirect dimension was set for rotor-synchronized data collection. Ten data points were collected in the indirect dimension. A recycle delay of 0.9 s was used for all MQMAS experiments. All ^{27}Al spectra were referenced to aqueous aluminum nitrate (0 ppm). All data were processed with the program RMN.[5] Line shape fitting of the ^{27}Al and ^{29}Si 1D MAS spectra was performed using the program DMFIT.[6]

Brønsted site densities were determined by isopropylamine (IPA, Acros, 99%) temperature programmed desorption (TPD).[7] Typically, 60-80 mg of sample was added into a 1/2 inch quartz tube between two quartz wool (Grace) end plugs. The tube was placed in an Omega furnace. The temperature of the furnace was regulated by a process controller (Love, series 16A) and monitored

by a type K thermocouple (Omega). All samples were calcined under air flow (50 sccm). A ramping protocol that prevents structural changes of the zeolites due to water evaporation was followed. The cell containing the samples was ramped to 373 (2 K min^{-1}) and was held at 373 K for 30 min. The cell was further heated at 393 K at the same rate and was held at 393 K for 30 min as well. Finally, the cell was ramped to 623 K (5 K min^{-1}) and was kept at that temperature for 300 min. The cell was subsequently cooled to 423 K, and purged in dry He flow (100 sccm) for more than 90 minutes. Catalysts were then dosed with isopropylamine in He flow. After saturation of IPA on the surface, He flow (400 sccm) removed physisorbed isopropylamine. The furnace temperature was then increased to 973K (10 K min^{-1}) under He including 1% Ar serving as an internal standard. Chemisorbed isopropylamine was converted into propene and ammonia during the temperature ramp. Throughout the entire process, a mass-selective residual gas detector (Stanford Instruments RGA 100) was used to track isopropylamine (m/z=44), propylene (m/z=41) and Ar (m/z=40) in the effluent. Evolved propylene was used to calculate Brønsted site density, assuming that one molecule of isopropylamine adsorbs per Brønsted site.

Brønsted acid sites to Lewis acid sites ratio was determined using pyridine Fourier transform infrared spectroscopy (FTIR, Nicolet 6700 DTGS detector). Approximately 15 mg of sample was pressed into a 13 mm pellet in a hydraulic press. The pellet was loaded into an in situ cell, designed and built in house. Catalysts were calcined as per the procedure described in the TPD experimental section. Subsequently, the cell was cooled to 423K, and purged under dry He flow (60 sccm). The pellet was then dosed with 4 torr of pyridine (Sigma Aldrich, 99%). After the pellet was fully saturated, the cell was purged under a He flow (200 sccm) at 423K to remove physisorbed pyridine. Spectra were collected at 423 K, and Brønsted to Lewis ratios were determined by the ratio of the integrated IR bands at 1545 cm^{-1} (pyridimium ion) and 1455 cm^{-1} (pyridine) respectively, by

applying the appropriate molar extinction coefficients.[8] Lewis site density was calculated from isopropylamine TPD and pyridine FTIR by the following equation: L=B/(B/L ratio).

1.4. Zeolite Degradation Rate Equation Derivation based on the Kirkwood Theory

Marrone et al. described the effect of water dielectric constant on the non-Arrhenius relationship governing dichloromethane hydrolysis in sub- and supercritical water. The dielectric constant varies from approximately 80.1 at room temperature to 1 at the critical point, as shown in Figure 8, meaning that it can exert a temperature-dependent effect on reactions which proceed via polar transition states. While dealumination and desilication transition states involved in zeolite degradation are not as well defined as their molecular analogs, previous computational analysis predicts that hydrolysis of Si−O and Al−O bonds proceeds via polarized transition states. A complete derivation of the underlying equations based on the Kirkwood theory is provided in the Supporting information and follows a similar methodology as Marrone et al.

Marrone et al. proposed combining Kirkwood dielectric continuum solvation theory with transition state theory to account for the temperature dependence of desilication and dealumination rates arising from the temperature dependence of the dielectric constant:

$$ln(k_{app}) = \ln(A) - \frac{E_A}{RT} + \Phi(T) \qquad (1)$$

where $\Phi(T)$ is the Kirkwood correlation factor. The Kirkwood correlation factor estimates the effects of the dielectric constant (ϵ_i) on the stabilization of the polar transition state for reactions of the type A + B →P, assuming that the solvent behaves as a continuum:

$$\Phi(T) = -\frac{1}{RT}\left(\left(\Delta G_{\epsilon}^{vac} - \Delta G_{\epsilon_a}^{vac}\right) + \frac{N_A}{4\pi\epsilon_0}\left(\frac{\epsilon_a - 1}{2\epsilon_a + 1}\left[\frac{\mu_{\ddagger,\epsilon_a}^2}{r_{\ddagger,\epsilon_a}^3} - \frac{\mu_A^2}{r_A^3} - \frac{\mu_B^2}{r_B^3}\right] - \frac{\epsilon - 1}{2\epsilon + 1}\left[\frac{\mu_{\ddagger,\epsilon}^2}{r_{\ddagger,\epsilon}^3} - \frac{\mu_A^2}{r_A^3} - \frac{\mu_B^2}{r_B^3}\right]\right)\right) \qquad (2)$$

where μ_i is the dipole moment r_i is the ionic radii (r_i) of either the reactant (denoted with the subscripts "A") the product (denoted with the subscript "B") or the transition state (denoted with $\neq$ subscript). In addition, ΔG_ϵ is the change in Gibbs free energy relative to vacuum and ϵ is the dielectric constant of water solvent. In a molecular reaction, equating ϵ with the bulk dielectric constant of the solvent is unambiguous. For reactions proceeding in molecular-scale micropores, the local value of the dielectric constant is less clear. In the case of desilication, which characterization data indicate occurs primarily at zeolite surfaces, using the bulk dielectric constant may be justified. For dealumination, which must occur primarily in the micropores themselves, using the bulk dielectric constant is less clear. However, no data are available to develop a model of the molecularly confined dielectric constant, meaning that no clear alternative is available. Accordingly, we used the bulk dielectric constant for analysis of both desilication and dealumination rates.

For this study, the dipole moments (μ_i), ionic radii (r_i) are considered to be weak functions of temperature, allowing them to be lumped together into a single factor, W:

$$\Phi(T) = -\frac{1}{RT}\left(\left(\Delta G_{\epsilon}^{vac} - \Delta G_{\epsilon_a}^{vac}\right) + W\left(\frac{\epsilon_a - 1}{2\epsilon_a + 1} - \frac{\epsilon - 1}{2\epsilon + 1}\right)\right) \quad (3)$$

Neglecting the temperature dependence of the dipole moments of the reactants is reasonable; Gubskaya and Kusalik indicate that the dipole of water varies only 10% over the range from 273 to 373 K. The temperature dependence of the transition state dipole is less clear; however, the present analysis must necessarily neglect it, as calculating the temperature dependent dipole moment of the Al−O and Si−O transition states is beyond the scope of this study. Instead, as with equating the micropore dielectric constant with the bulk value, we sought to determine if Kirkwood theory, when combined with the bulk dielectric constant of water, has the correct form for empirical description of desilication and dealumination rates. By combining

2. Nitrogen Sorption

Nitrogen sorption was used to investigate the effects of liquid water treatment on ZSM-5 surface area and micro/meso-porosity. Compared to STEM, nitrogen sorption is a bulk technique that accounts for the porosity of the entire sample. **Figure SI-1** shows that the measured isotherms were consistent with IUPAC type II [12] characteristic of a microporous material. Nitrogen sorption isotherms of this type can be divided into 2 main regions, depending on the pressure (P/P_0). For $P/P_0 < 10^{-3}$, the isotherm is associated with gas-zeolite interactions within micropores. For $P/P_0 > 0.1$ the isotherm is associated with gas-gas molecular interactions within mesopores; in particular, curvature of the sorption isotherm for $P/P_0 > 0.1$ is attributable to mesoporosity. Qualitatively, the sorption isotherm of the parent ZSM-5 indicates that the majority of adsorption occurs in the low pressure region, with modest adsorption at $P/P_0 > 0.1$ consistent with a microporous solid lacking mesoporosity.[13] After treatment in hot liquid water, curvature in the pressure range of $P/P_0 = 0.1$-1.0 increases slightly, with evidence of minor adsorption-desorption hysteresis. A large increase of the curvature in the mesopore range has been attributed to ZSM-5 de-silication[14,15] from alkaline treatment. The minor changes in the adsorption isotherms of treated ZSM-5 indicate that the framework remains largely microporous (>90%) with only modest mesopore formation. These observations are consistent with the STEM images shown in Figure 3.

The abundant literature on zeolite degradation under acidic and basic[15–21] conditions can provide insight on the trends observed in the N_2 sorption isotherms. Base catalysis by OH^- selectively cleaves siloxane framework bonds, leading to de-silication.[15,17–21] Desilication of a zeolite in an alkaline medium will often initiate at internal sites[20] and propagate from hydroxyl nest defects introduced into the framework during synthesis or dealumination.[18,19,22,23] The extent of zeolite desilication greatly depends on the zeolite structure and its Si/Al ratio.[24] The end result of base

catalyzed desilication is increased curvature of the N_2 isotherm for $P/P_0 > 0.1$ and increased mesoporosity. This is the typical observation made of zeolites exposed to hot liquid water conditions, including H-β[25] and H-Y[26]. In contrast to base catalyzed desilication, numerous studies report that acids promote zeolite dealumination,[18,19,33,34,21,24,27–32] with minimal framework degradation. In acid solutions, dealumination occurs via a proton/hydronium catalyzed mechanism that selectively removes Al sites, forming a variety of extra-framework hydroxyaluminate complexes that impart Lewis acidity as well as mono, di and/or trivalent Al cations.[24] The modest isotherm changes observed for liquid-treated ZSM-5 closely mirror those reported for acid-treated zeolites,[14,18,35] Dealumination of ZSM-5 could be consistent with the observation of Gardner et al.[36] that exposure of ZSM-5 to liquid water at 150 °C results in increased concentration of Al species in the water solution.

The final feature present in the gas sorption isotherms that merits discussion is the substep observed at approximately $P/P_0 = 0.1$ for ZSM-5 treated in liquid water at 430 and 450 °C. Minor qualitative differences were present in the isotherms of treated ZSM-5, specifically a minor change in the curvature of the isotherm in the mesopore region, which is consistent with retention of a structure dominated by micropores, and a minor substep in samples treated at 430 and 450 °C; the substep has sometimes been attributed to dealumination.[35,37]Saito et al.[37] reported that a step in the N_2 isotherm appears and becomes more prominent as the Si/Al ratio of ZSM-5 increases. They attributed the observed phenomena to a fluid to solid transition of N_2 adsorbate.[37] The substep is less pronounced when aluminum is incorporated into the framework, which contributes electrostatic effects that cause surface energy heterogeneity that dampens the substep.[37] More specifically, Triantafillidis et al.[35] identified a similar substep for ZSM-5 with a Si/Al ratio >1000 and in ZSM-5 with an initial ratio Si/Al of 26.5 that was steamed at 790 °C for 6 hours to

dealuminate the framework. In contrast, Triantafillidis et al.[35] did not observe a sub-step for ZSM-5 with Si/Al =27. As with the previous study,[35] the parent ZSM-5 (Si/Al = 38) did not exhibit a sub-step, whereas the liquid treated samples do. As with the other features of the N_2 adsorption curve and some of the features of the XRD spectra, the presence of a sub-step in the treated samples is therefore consistent with dealumination.

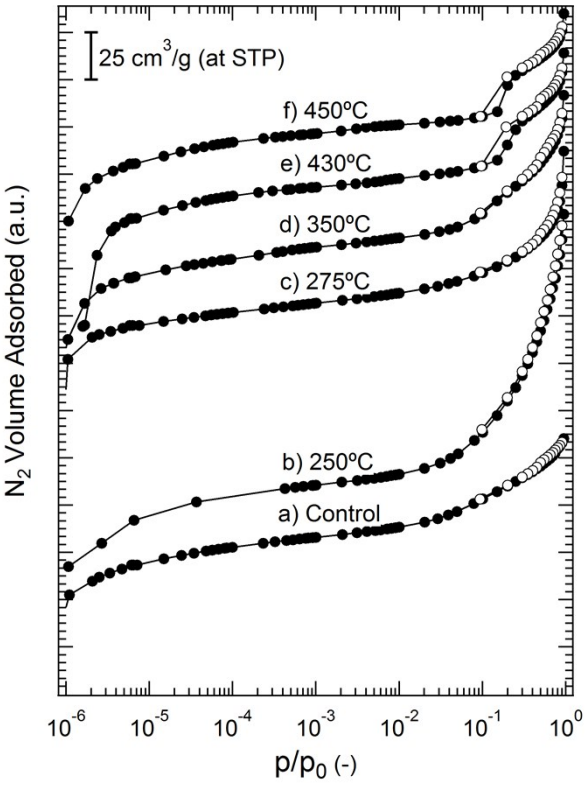

Figure SI-1. H-ZSM5 nitrogen sorption isotherms for a) untreated, b) 250 °C treated, c) 275 °C treated, d) 350 °C treated, e) 430 °C treated, and f) 450 °C treated samples in hot liquid water

The main text provides evidence of changes to ZSM-5 crystallinity and textural properties during exposure to HLW and SCW. Inter-comparison of ZSM-5 crystallinity, surface area, and pore volume reveals a complex relationship between framework and surface area stability of treated ZSM-5. **Figure SI-2** plots surface area determined from N_2 sorption as a function of measured crystallinity. Total surface area, external surface area, and micropore area are all plotted as separate

traces, and marker size are both labeled and rated to treatment temperature. Interestingly, in all cases, the relationship between crystallinity and surface area is complicated and non-monotonic. As a general trend, modest decreases in crystallinity (2-5%) lead to increases in surface area. Crystallinity decreases of 5-10% result in much larger decreases in surface area, ranging from 10-40%. For further decreases in crystallinity of more than 10% the surface area remains nearly constant at the values obtained for 5-10% decreases in crystallinity. Lastly, the effect of temperature is complex, with all of the trends exhibiting non-monotonic relationships with temperature. These data help show the complexity of the changes in surface area and crystallinity of HLW and SCW treated ZSM-5.

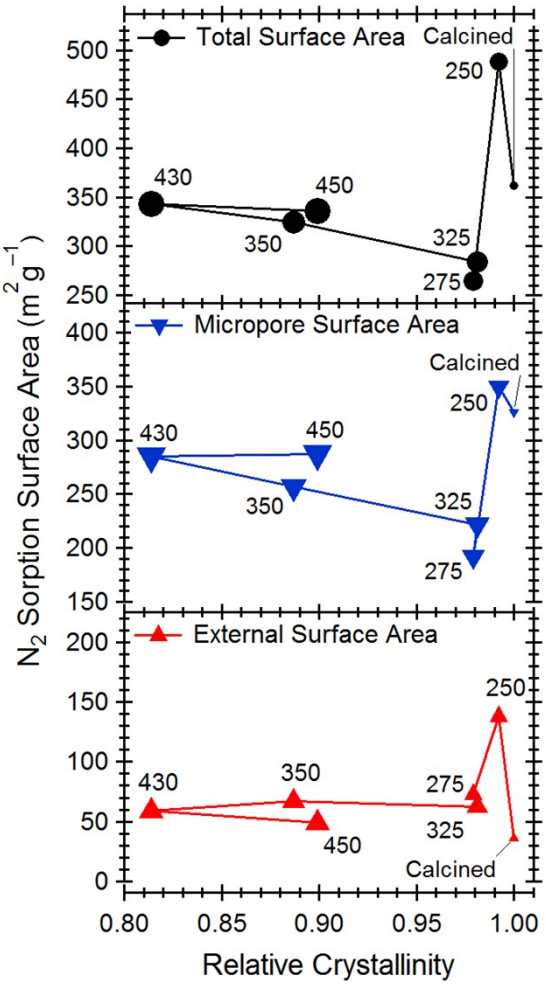

Figure SI-2. Comparison of textural properties relative to the degree of crystallinity of hot liquid water treated ZSM-5. Textural properties are calculated from N_2 isotherms, including micropore area (blue triangle), external surface area (red triangle) and total surface area (black circle). Relative crystallinity is obtained based on XRD diffractograms. Marker size is rated to treatment temperature. Untreated ZSM5 samples are denoted with a star point and are labeled.

3. NMR Analysis

^{29}Si NMR was used to determine elemental connectivity and coordination of the silicon atoms present in ZSM-5. **Figure SI-3** shows ^{29}Si NMR spectra fitted with Gaussian peaks for both ZSM-5 calcined powders and treated in hot liquid water. Considering first the calcined sample (**Figure SI-3a**), the spectrum is fit with three distinct Gaussian curves with chemical shifts ($^{Si}\delta$) located at −116, −112 and −107 ppm. Peaks located at −116 and −112 ppm are assigned to Si atoms with 4 Si neighbors in their second coordination sphere (Q_4 sites), while the −107 ppm peak is assigned to Si atoms with 3 Si neighbors and either an Al atom or hydroxyl group in its second coordination sphere (Q_3 sites).[38]

^{29}Si NMR of the treated samples are consistent with dealumination inferred from DRIFTS and XPS analysis. **Figures SI-3b-d** show ^{29}Si NMR spectra of the treated samples. Focusing first on qualitative features, the ^{29}Si NMR spectrum of ZSM-5 treated at 250 °C (**Figure SI-3b**) indicates only modest changes relative to the calcined sample, with a minor increase of the intensity of the Q_4 band at −116 ppm. The minor changes observed in the ^{29}Si NMR spectrum of ZSM-5 treated at 250 °C relative to the calcined version are consistent with the stability of the sample at these conditions indicated by XRD and microscopy. The intensity the Q_3 peak decreases after treatment at 325 °C and the peaks associated with Q_4 sites narrow (**Figure SI-3c**). Narrowing of Q_4 peaks has been reported in studies of steam dealumination ZSM-5.[34,39] Peaks in the ^{29}Si NMR spectra of

ZSM-5 treated at 400 °C (**Figure SI-3d**) are increasingly narrow; in fact, the spectra of ZSM-5 treated at 400 and 450 °C resemble silicalite,[39] suggesting near quantitative removal of Al atoms from the framework. Lastly, a new peak located at −92 ppm appears in the spectra of samples treated at 400 and 450 °C. This peak is attributed to Q_2 sites associated with Al-O-Si-O-Al bonding configuration with each aluminum in a tetrahedral coordination.[39] Although tetrahedral aluminum sites are typically associated with framework aluminum, Ong et al.[29] has identified possible tetrahedral configurations for EFAL within steamed ZSM-5 that associate near framework aluminum sites. Again, all indications from the ^{29}Si NMR support dealumination of ZSM-5 under hot liquid water conditions.

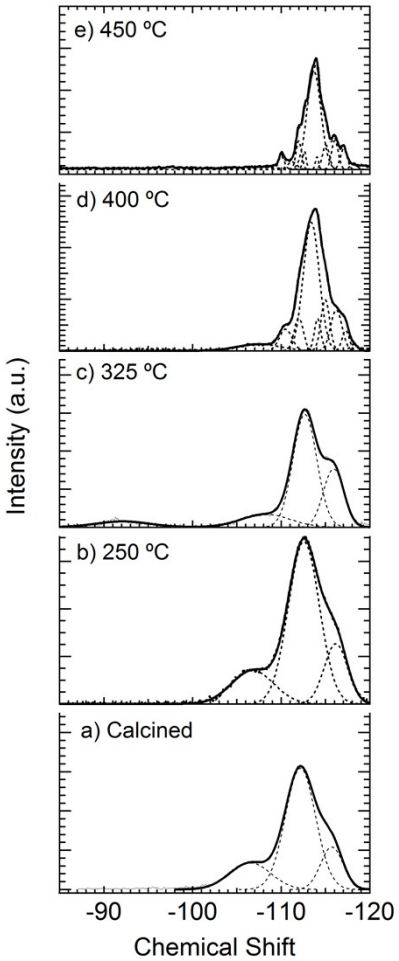

Figure SI-3. 1-D ^{29}Si NMR spectra for a) untreated, b) 250 °C treated c) 325 °C treated, d) 400 °C treated, and e) 450 °C treated samples in hot liquid water.

The ^{27}Al NMR spectra shown in main text contains peaks that can be assigned to both tetrahedrally coordinated framework aluminum and octahedrally coordinated extra-framework aluminum species. In addition to these Al species, the spectra contain a contribution from the aluminum rotor, which is centered at 10 ppm that does not arise from the sample itself. The rotor peak is more easily observable as the 2D Al MQMAS spectra shown in **Figure SI-4**. The peak centered at F2 = 10 ppm is distinctly separate from the tetrahedral and octahedral oriented species in all 5 2D Al MQMAS plots (**Figures SI-4a to e**). The untreated sample plotted in **Figure SI-4a** shows that the framework aluminum peak centered at F2 = 50 ppm is the main species for ZSM-5 and the contribution of the rotor is expectedly small. Upon increasing hot liquid water treatment temperatures, the relative rotor contribution increases as ZSM-5 dealuminates and becomes relatively more siliceous. The rotor contribution in **Figure SI-4e** (ZSM-5 treated at 450 °C) is the primary feature of the MQMAS spectra only as this sample lacks both framework and extra-framework aluminum species.

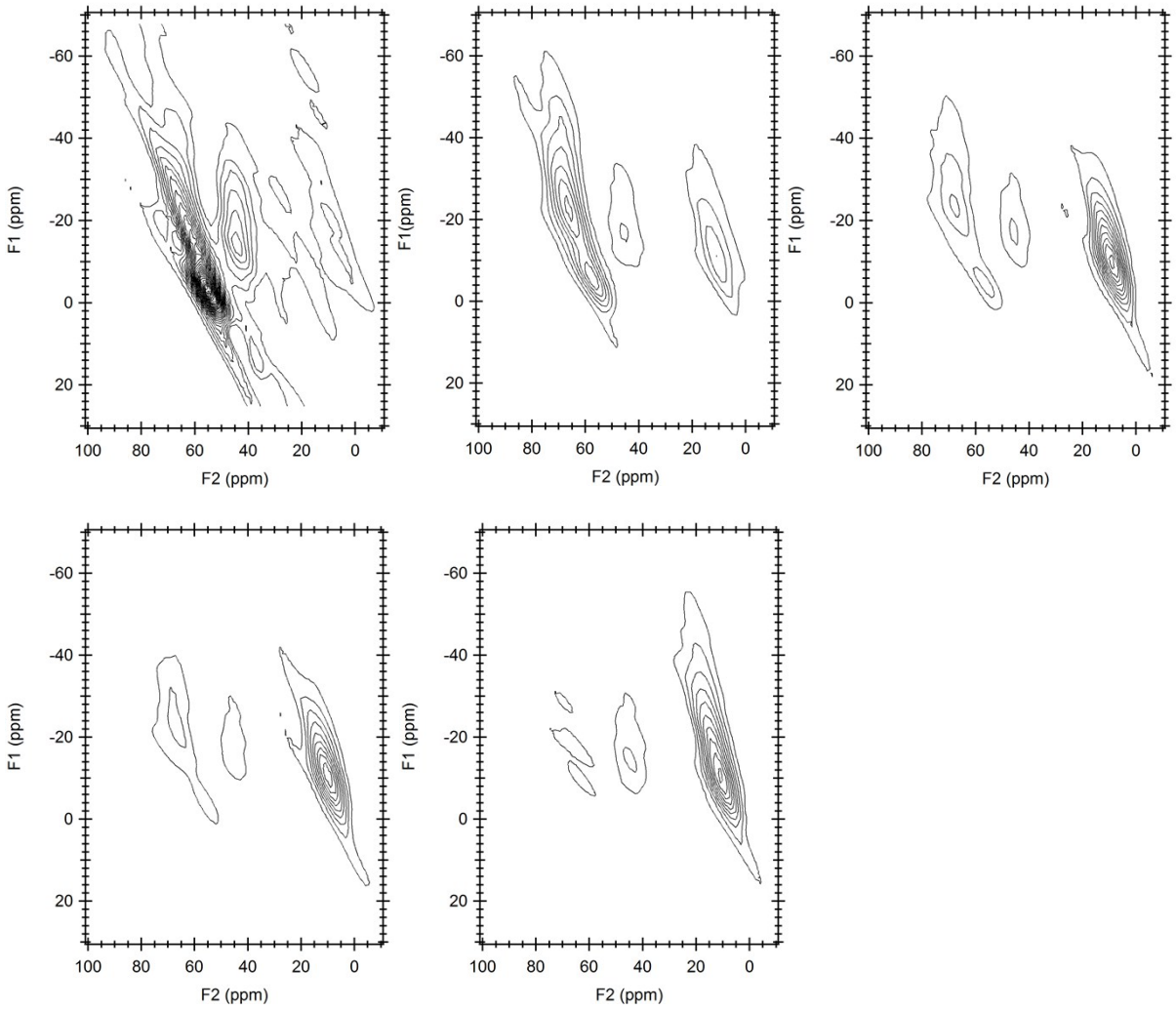

Figure SI-4. 2D Al NMR: 2-D ^{27}Al NMR spectra for a) Calcined, b) 250°C treated, c) 325°C treated, d) 400°C and e) 450°C treated samples in hot liquid water.

4. Scanning electron microscopy with energy dispersive x-ray spectroscopy (SEM-EDS)

EDS was used to determine if the surface features observed in the SEM images (Figure 2 in the main text) were composed of amorphous silica, amorphous alumina, or a crystalline silicate with composition similar to ZSM-5. **Figure SI-5** shows representative EDS images of calcined ZSM-5 (**Figure SI-5a**), ZSM-5 treated in hot liquid water at 250 °C (**Figure SI-5b**), ZSM-5 treated in hot

liquid water at 325 °C (**Figure SI-5c**) and ZSM-5 treated in hot liquid water at 450 °C (Figure SI-2d). As expected, **Figure SI-5a** shows uniform Al distribution on the surfaces of calcined ZSM-5. In contrast, the Al distribution on the surfaces of samples treated at 250 and 325 °C is non-uniform, exhibiting distinct regions of enhanced Al content (**Figures SI-5b and c**). The surface Al distribution of the sample treated at 450 °C (**Figure SI-5d**) is more uniform than the surfaces of ZSM-5 treated at 250 and 325 °C, lacking the regions of distinct Al enrichment. **Figure SI-5** indicates that dealumination results in agglomerated alumina regions at temperatures equal to or less than 325 °C but not at 450 °C, possibly indicative of different mechanisms at the different conditions.

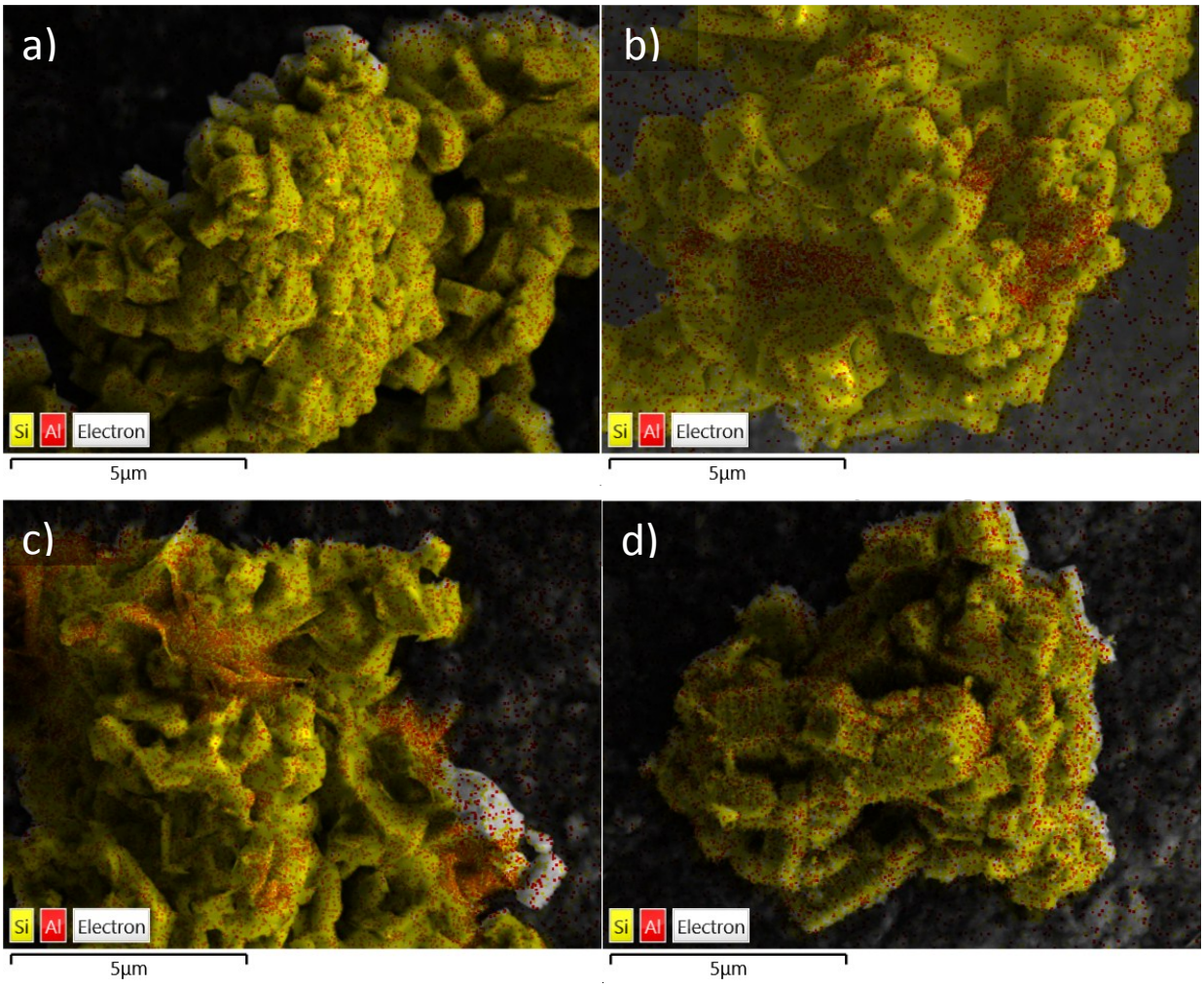

Figure SI-5. SEM-EDS images of ZSM-5 samples a) untreated, b) 250 °C b) 325 °C and d) 450 °C treated samples in hot liquid water.

5. Pyridine Infrared Spectroscopy

The stacked pyridine IR spectra displayed in **Figure SI-6** were performed to compare the relative amount of Bronsted acid sites (BAS) to Lewis acid sites (LAS) of calcined and HLW treated ZSM-5 samples. The FTIR spectra of pyridine-adsorbed ZSM-5 are similar to others reported in the literature,[40–42] with no major qualitative differences between calcined ZSM-5 and materials treated in liquid water. Bands associated with Brønsted and Lewis acids were integrated to estimate the ratio of the two acid types in ZSM-5. Specifically, the peak areas for stretching modes located at 1450 cm^{-1} and 1545 cm^{-1} are used to quantify the relative amount of LAS and BAS respectively and obtain a Brønsted to Lewis ratio (B/L ratio). The B/L ratio of calcined ZSM-5 is calculated to be 9.8; an expected result for synthesized ZSM-5 which is predominately Bronsted acidic. Upon HLW treatment at 350 °C, the B/L decreases to 3.8, which is likely due to contibuting factors of BAS loss and the corresponding formation of LAS species such as extra framework alumina. When ZSM-5 is treated in 450 °C HLW, the B/L ratio continues to decrease, consistent with a continual loss in BAS with increasing temperature. Unlike ZSM-5 observed changes in framework degradation that vary with temperature dependant solvent effects, BAS density decreases monotonically with increasing temperature. The spectra shown in **Figure SI-6** were used for the quantitative data provided in Table 2 in the main text.

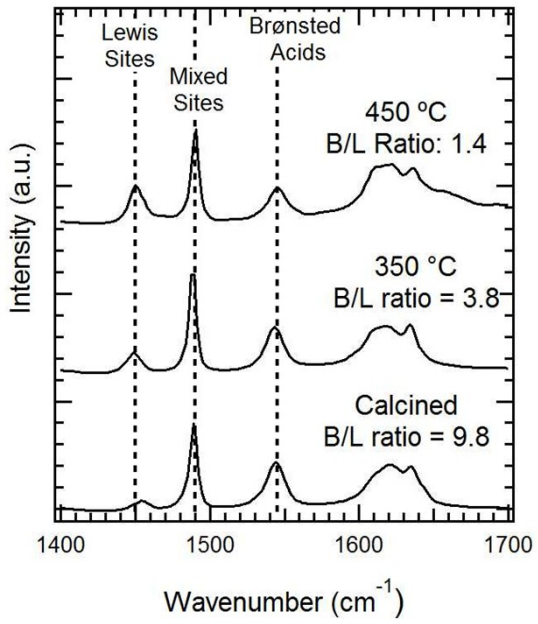

Figure SI-6. Pyridine IR Spectra of untreated H-ZSM5 samples compared to samples treated in either 350 or 450 °C hot liquid water conditions. Calculated Brønsted to Lewis acid ratios (B/L ratio) are included in the figure.

7. Kinetic analysis of literature studies on degradation of MFI and other zeolite frameworks

Ravenelle et al.[11] obtained temporal data on the crystallinity loss of HY after hot liquid water treatment that follows a first-order degradation kinetics. This can be shown by transforming the temporal data obtained from their study into a first-order rate analysis:

$$ln\left[\frac{CI(t)}{CI(t=0)}\right] = -k_{app}t \qquad (4)$$

Experimental crystallinity were fit to estimate the apparent rate desilication rate constant, k_{app}, at different temperatures. The plot of the natural log of relative CI over time for HY from Ravenelle et al.[11] is provided in Figure SI-9. The first-order plot shown in Figure SI-9 is clearly linear, confirming the framework degradation rate law is first order.

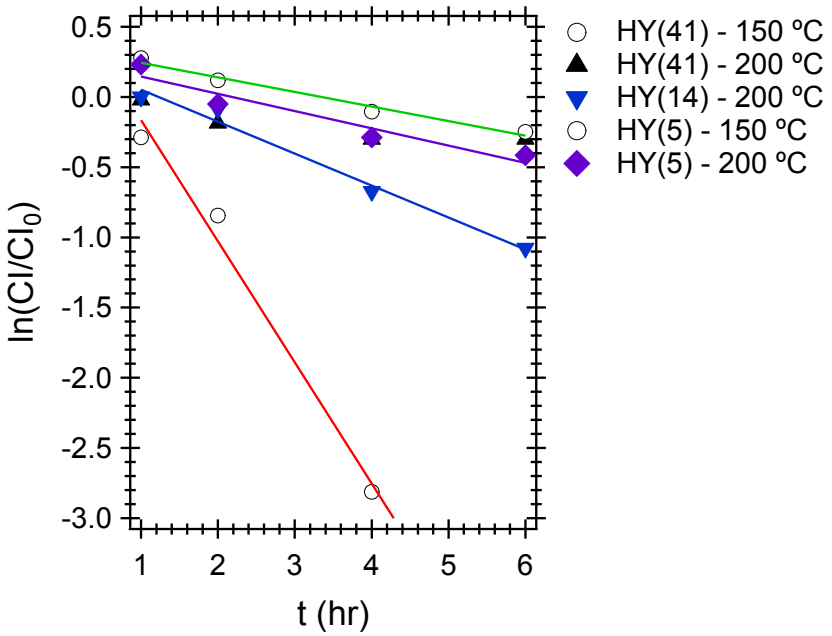

Figure SI-7. First order rate plot of HY degradation under hot liquid water conditions (natural log of the relative retained crystallinity (CI/CI_0) versus time). Data points are denoted in the legend with their corresponding Si/Al ratios in parenthesis followed by treatment temperature.

Experimental data obtained for ZSM-5 decrystallization (XRD) and dealumination (NMR) were then analyzed to determine values of k_{app} over the temperature range from 250 to 450 °C. Table SI-1 provides the numerical values, which are used in the analysis shown in Figure 7.

Table SI-1. Degradation rate constants for both ZSM-5 decrystallization and dealumination

Temperature (°C)	Decrystallization k_{app} (XRD) [a]	Dealumination k_{app} (NMR) [b]
250	-14.16	-8.86
275	-13.15	-8.81
325	-13.26	-9.44
350	-11.41	N/A
400	-10.93	-8.18
425	-10.88	N/A
430	-10.87	-8.41
440	-11.98	-7.89
450	-11.52	-8.23

[a] Decrystallization rate constant obtained based on retained crystallinity values from XRD;
[b] Dealumination rate constant obtained based on the ratio of tetrahedral to octahedral acid sites from both ^{29}Si and ^{27}Al NMR

References

1. ASTM. *Standard Test Method for Determination of Relative Crystallinity of Zeolite ZSM-5 by X-Ray Diffraction*. *ASTM International: D4758-01* **05,** (2015).

2. Wagner, C. D. *et al.* Empirical atomic sensitivity factors for quantitative analysis by electron spectroscopy for chemical analysis. *Surf. Interface Anal.* **3,** 211–225 (1981).

3. Aliev, A. E., Harris, K. D. M. & Apperley, D. C. Natural abundance high-resolution solid state 2H NMR spectroscopy. *Chem. Phys. Lett.* **226,** 193–198 (1994).

4. Madhu, P. ., Goldbourt, A., Frydman, L. & Vega, S. Sensitivity enhancement of the MQMAS NMR experiment by fast amplitude modulation of the pulses. *Chem. Phys. Lett.* **307,** 41–47 (1999).

5. Grandinetti, P. RMN, Version 1.3.0; The Ohio State University: Columbus, OH,. (2005).

6. Massiot, D. *et al.* Modelling one- and two-dimensional solid-state NMR spectra. *Magn. Reson. Chem.* **40,** 70–76 (2002).

7. Tittensor, J. G., Gorte, R. J. & Chapman, D. M. Isopropylamine adsorption for the characterization of acid sites in silica-alumina catalysts. *J. Catal.* **138,** 714–720 (1992).

8. Emeis, C. A. Determination of Integrated Molar Extinction Coefficients for Infrared Absorption Bands of Pyridine Adsorbed on Solid Acid Catalysts. *J. Catal.* **141,** 347–354 (1993).

9. Lutz, W., Toufar, H., Kurzhals, R. & Suckow, M. Investigation and modeling of the hydrothermal stability of technically relevant zeolites. *Adsorption* **11,** 405–413 (2005).

10. Vjunov, A. *et al.* Impact of aqueous medium on zeolite framework integrity. *Chem. Mater.* **27,** 3533–3545 (2015).

11. Ravenelle, R. M. *et al.* Stability of zeolites in hot liquid water. *J. Phys. Chem. C* **114,** 19582–19595 (2010).

12. Donohue, M. . & Aranovich, G. . Classification of Gibbs adsorption isotherms. *Adv. Colloid Interface Sci.* **76,** 137–152 (1998).

13. Groen, J. C., Peffer, L. A. A. & Pérez-Ramírez, J. Pore size determination in modified micro- and mesoporous materials. Pitfalls and limitations in gas adsorption data analysis. *Microporous Mesoporous Mater.* **60,** 1–17 (2003).

14. You, S. J. & Park, E. D. Effects of dealumination and desilication of H-ZSM-5 on xylose dehydration. *Microporous Mesoporous Mater.* **186,** 121–129 (2014).

15. Groen, J. C., Peffer, L. A. A., Moulijn, J. A. & Pérez-Ramírez, J. Mesoporosity development in ZSM-5 zeolite upon optimized desilication conditions in alkaline medium. *Colloids Surfaces A Physicochem. Eng. Asp.* **241,** 53–58 (2004).

16. Fodor, D., Krumeich, F., Hauert, R. & Van Bokhoven, J. A. Differences between individual ZSM-5 crystals in forming hollow single crystals and mesopores during base leaching. *Chem. - A Eur. J.* **21,** 6272–6277 (2015).

17. Groen, J. C., Jansen, J. C., Moulijn, J. A. & Pérez-Ramírez, J. Optimal aluminum-assisted mesoporosity development in MFI zeolites by desilication. *J. Phys. Chem. B* **108,** 13062–13065 (2004).

18. Groen, J. C., Moulijn, J. A. & Pérez-Ramírez, J. Decoupling mesoporosity formation and acidity modification in ZSM-5 zeolites by sequential desilication-dealumination. *Microporous Mesoporous Mater.* **87,** 153–161 (2005).

19. Groen, J. C., Peffer, L. A. A., Moulijn, J. A. & Pérez-Ramírez, J. Mechanism of hierarchical porosity development in MFI zeolites by desilication: The role of aluminium as a pore-directing agent. *Chem. - A Eur. J.* **11,** 4983–4994 (2005).

20. Verboekend, D. & Pérez-Ramírez, J. Design of hierarchical zeolite catalysts by desilication. *Catal. Sci. Technol.* **1,** 879 (2011).

21. van Donk, S., Janssen, A. H., Bitter, J. H. & de Jong, K. P. Generation, Characterization, and

Impact of Mesopores in Zeolite Catalysts. *Catal. Rev.* **45,** 297–319 (2003).

22. Zhang, L., Chen, K., Chen, B., White, J. L. & Resasco, D. E. Factors that Determine Zeolite Stability in Hot Liquid Water. *J. Am. Chem. Soc.* **137,** 11810–11819 (2015).

23. Abelló, S., Bonilla, A. & Pérez-Ramírez, J. Mesoporous ZSM-5 zeolite catalysts prepared by desilication with organic hydroxides and comparison with NaOH leaching. *Appl. Catal. A Gen.* **364,** 191–198 (2009).

24. Silaghi, M. C., Chizallet, C. & Raybaud, P. Challenges on molecular aspects of dealumination and desilication of zeolites. *Microporous Mesoporous Mater.* **191,** 82–96 (2014).

25. Prodinger, S. *et al.* Improving Stability of Zeolites in Aqueous Phase via Selective Removal of Structural Defects. *J. Am. Chem. Soc.* jacs.5b12785 (2016). doi:10.1021/jacs.5b12785

26. Zapata, P. A., Huang, Y., Gonzalez-Borja, M. A. & Resasco, D. E. Silylated hydrophobic zeolites with enhanced tolerance to hot liquid water. *J. Catal.* **308,** 82–97 (2013).

27. Beyerlein, R. a, Choi-feng, C., Hall, J. B., Huggins, B. J. & Ray, G. J. Effect of steaming on the defect structure and acid catalysis of protonated zeolites. *Top. Catal.* **4,** 27–42 (1997).

28. Nielsen, M. *et al.* Kinetics of Zeolite Dealumination: Insights from H-SSZ-13. *ACS Catal.* **5,** 7131–7139 (2015).

29. Ong, L. H., Dömök, M., Olindo, R., Van Veen, A. C. & Lercher, J. A. Dealumination of HZSM-5 via steam-treatment. *Microporous Mesoporous Mater.* **164,** 9–20 (2012).

30. Triantafillidis, C. S., Vlessidis, A. G. & Evmiridis, N. P. Dealuminated H−Y Zeolites: Influence of the Degree and the Type of Dealumination Method on the Structural and Acidic Characteristics of H−Y Zeolites. *Ind. Eng. Chem. Res.* **39,** 307–319 (2000).

31. Masuda, T., Fujikata, Y., Mukai, S. R. & Hashimoto, K. Changes in catalytic activity of MFI-type zeolites caused by dealumination in a steam atmosphere. *Appl. Catal. A Gen.* **172,** 73–83 (1998).

32. Valtchev, V., Majano, G., Mintova, S. & Pérez-Ramírez, J. Tailored crystalline microporous materials by post-synthesis modification. *Chem. Soc. Rev.* **42,** 263–290 (2013).

33. Maier, S. M., Jentys, A. & Lercher, J. A. Steaming of zeolite BEA and its effect on acidity: A comparative NMR and IR spectroscopic study. *J. Phys. Chem. C* **115,** 8005–8013 (2011).

34. Niwa, M., Sota, S. & Katada, N. Strong Brønsted acid site in HZSM-5 created by mild steaming. *Catal. Today* **185,** 17–24 (2012).

35. Triantafillidis, C. S., Vlessidis, A. G., Nalbandian, L. & Evmiridis, N. P. Effect of the degree and type of the dealumination method on the structural, compositional and acidic characteristics of H-ZSM-5 zeolites. *Microporous Mesoporous Mater.* **47,** 369–388 (2001).

36. Gardner, D. W. *et al.* Insights into the Hydrothermal Stability of ZSM-5 under Relevant Biomass Conversion Reaction Conditions. *ACS Catal.* **5,** 4418–4422 (2015).

37. Saito, A. & Foley, H. C. High-resolution nitrogen and argon adsorption on ZSM-5 zeolites: effects of cation exchange and Si Al ratio. *Microporous Mater.* **3,** 543–556 (1995).

38. Maijanen, A., Derouane, E. & Nagy, J. FT-IR and solid-state NMR investigation of surface hydroxyl groups on dealuminated ZSM-5. *Appl. Surf. Sci.* 204–212 (1994). doi:10.1017/CBO9781107415324.004

39. Fyfe, C. a, Gobbi, G. C. & Kennedy, G. J. Investigation of the conversion (dealumination) of ZSM-5 into silicalite by high-resolution solid-state 29Si and 27Al MAS NMR spectroscopy. *J. Phys. Chem.* **88,** 3248–3253 (1984).

40. Rahimi, N. & Karimzadeh, R. Catalytic cracking of hydrocarbons over modified ZSM-5 zeolites to produce light olefins: A review. *Appl. Catal. A Gen.* **398,** 1–17 (2011).

41. Serrano, D. P., García, R. A., Linares, M. & Gil, B. Influence of the calcination treatment on the catalytic properties of hierarchical ZSM-5. *Catal. Today* **179,** 91–101 (2012).

42. Jin, F. & Li, Y. A FTIR and TPD examination of the distributive properties of acid sites on ZSM-5 zeolite with pyridine as a probe molecule. *Catal. Today* **145,** 101–107 (2009).

43. Karásek, P., Šťavíková, L., Planeta, J., Hohnová, B. & Roth, M. Solubility of fused silica in sub- and supercritical water: Estimation from a thermodynamic model. *J. Supercrit. Fluids* **83,** 72–77 (2013).

44. Dolejš, D. & Manning, C. E. Thermodynamic Model for Mineral Solubility in Aqueous Fluids: Theory, Calibration and Application to Model Fluid-Flow Systems. *Front. Geofluids* 20–40 (2011). doi:10.1002/9781444394900.ch3